

1 **Solid/CO<sub>2</sub> and solid/water interfacial tensions as a function of pressure, temperature,**  
2 **salinity and mineral type: Implications for CO<sub>2</sub>-wettability and CO<sub>2</sub> geo-storage**

3  
4 Muhammad Arif<sup>1,\*</sup>, Ahmed Barifcani<sup>1</sup>, Stefan Iglauer<sup>1</sup>

5  
6 <sup>1</sup>Curtin University, Department of Petroleum Engineering, 26 Dick Perry Avenue, 6151  
7 Kensington, Western Australia; phone: +61 8 9266 7703

8  
9 \*Corresponding author

10 Phone: +61 8 9266 7703

11 Fax: +61 8 9266 7063

12 Email: muhammad.arif@curtin.edu.au

13  
14  
15 **Abstract:**

16  
17 Wettability of CO<sub>2</sub>/brine/mineral systems plays a significant role in the underground geological  
18 storage of CO<sub>2</sub> as it governs the fluid flow and distribution mechanism within the porous  
19 medium. Technically, wettability is influenced by CO<sub>2</sub> pressure, the temperature of the storage  
20 formation, formation water salinity and the type of mineral under investigation. Although a  
21 growing number of studies report wettability data for CO<sub>2</sub>/water/mineral systems, yet the  
22 factors responsible for wettability variation with pressure and temperature remain unclear. In  
23 this work, we used the concept of surface energy to explain dependency of wettability on  
24 pressure, temperature and salinity. Neumann's equation of state approach was used to compute  
25 solid/CO<sub>2</sub> and solid/water interfacial energies using reliable contact angle and CO<sub>2</sub>/brine  
26 interfacial tension data from the literature at a wide range of operating conditions for quartz,  
27 water-wet mica, oil-wet mica and high, medium and low-rank coals. Moreover, the all-  
28 important question that why different minerals offer different wettability to CO<sub>2</sub>/water systems  
29 at the same pressure and temperature of investigation is addressed by comparing the interfacial  
30 energies of the minerals. We found that for all minerals solid/CO<sub>2</sub> interfacial energy decreased  
31 with pressure and increased with temperature, and solid/water interfacial energy decreased with  
32 temperature except for quartz for which solid/water interfacial energy increased with  
33 temperature. Furthermore, the solid/CO<sub>2</sub> interfacial energy was lowest for the oil-wet mica

34 surface and highest for quartz which is due to higher hydrophobicity of oil-wet mica surface.  
35 The results of the study lead to a better understanding of the wetting phenomenon at the  
36 CO<sub>2</sub>/brine/mineral interface and thus contribute towards the better evaluation of geological  
37 CO<sub>2</sub>-storage processes.

38

## 39 **1. Introduction**

40 Carbon capture and storage in depleted hydrocarbon reservoirs or deep saline aquifers  
41 contributes significantly towards the reduction of anthropogenic greenhouse gas emissions  
42 (Intergovernmental Panel on Climate Change, 2005). CO<sub>2</sub> is also injected into subsurface  
43 reservoirs for enhanced oil and gas recovery (e.g. Blunt et al., 1993; Iglauer et al., 2013, 2016;  
44 Lackner, 2003). In this context the wettability of CO<sub>2</sub>-brine-mineral systems plays a crucial  
45 role in deciding the fate of the injected CO<sub>2</sub> within the geological formation (Iglauer et al.,  
46 2015a). The existing literature has reported experimental CO<sub>2</sub>-wettability data as a function of  
47 pressure, temperature and salinity for rock forming minerals such as quartz (Al-Yaseri et al.,  
48 2016a; Saraji et al., 2014; Sarmadivaleh et al., 2015), mica (Arif et al., 2016a, b; Broseta et al.,  
49 2012; Chiquet et al., 2007) and coals (Arif et al., 2016c; Shojai Kaveh et al., 2012; Siemons et  
50 al., 2006). Further, molecular dynamics simulations also computed contact angles for CO<sub>2</sub>-  
51 brine-quartz systems (Chen et al., 2015; Iglauer et al., 2012; Javanbakht et al., 2015; Liu et al.,  
52 2010; McCaughan et al., 2013). However, no significant attention has been given to evaluate  
53 the factors which are responsible for wettability variation with pressure, temperature and  
54 salinity despite the variations in trends observed in studies on CO<sub>2</sub> wettability of minerals (e.g.  
55  $\theta$  increased in temperature for quartz/CO<sub>2</sub>/brine, Al-Yaseri et al., 2016a and decreased with  
56 temperature for mica/CO<sub>2</sub>/brine and coal/CO<sub>2</sub>/brine systems, Arif et al., 2016a,c).

57

58 Recently, a few studies attempted to explain the factors responsible for wettability variation.  
59 For instance, Al-Yaseri et al. (2016b) reported that wettability of quartz/gas/brine systems is a  
60 strong function of gas density and a mathematical correlation was developed to determine  
61 contact angles from gas densities. However, the methodology was applicable to a limited set  
62 of operating conditions only. Roshan et al. (2016) developed a physical model based the  
63 concept of the diffuse double layer to provide a theoretical framework for changes observed in  
64 wettability as a function of pressure, temperature and salinity and found that wettability is  
65 strongly related to CO<sub>2</sub>/water interfacial tensions and density changes. Ameri et al. (2013)  
66 computed sandstone/CO<sub>2</sub> interfacial tension as a function of pressure using Neumann's  
67 equation of state (Neumann et al., 1974) and found that the solid/CO<sub>2</sub> interfacial tension

68 decreased with pressure and they formulated that such change in solid surface energy is  
69 responsible for wettability changes. Nevertheless, the factors responsible for wettability  
70 variation with pressure, temperature and salinity remain unclear and require further attention.  
71 Theoretically, it is well-established that the contact angle is a function of the interplay of the  
72 three interfacial tensions (solid/CO<sub>2</sub>, solid/brine and brine/CO<sub>2</sub>) as related by Young-Laplace  
73 equation below:

$$74 \quad \cos\theta = \frac{\gamma_{sc} - \gamma_{sw}}{\gamma_{cw}} \quad (1)$$

75 In equation (1),  $\gamma_{sc}$ ,  $\gamma_{sw}$  and  $\gamma_{cw}$  denote solid/CO<sub>2</sub>, solid/water and CO<sub>2</sub>/water interfacial tensions  
76 respectively. To assess the wettability dependence on these interfacial interactions, the  
77 quantification of the three interfacial tensions ( $\gamma_{sc}$ ,  $\gamma_{sw}$  and  $\gamma_{cw}$ ) is essential. In this context,  
78 CO<sub>2</sub>/water interfacial tensions ( $\gamma_{cw}$ ) can be determined experimentally (many studies reported  
79 this data e.g. Arif et al., 2016a; Li et al., 2012; Lun et al., 2012), however, an independent  
80 experimental measurement of solid/fluid interfacial tension is not possible because a solid  
81 interface is very different from a fluid-fluid interface due to absence of mobility (Li and  
82 Neumann, 1992). Consequently, the use of numerical/empirical techniques such as Neumann's  
83 equation of state becomes essential (Neumann et al., 1974). They applied this method to  
84 compute surface energies of low energy polymers (Neumann et al., 1974, Kwok and Neumann,  
85 1999). We, thus, extend the use of Neumann's equation of state to compute mineral/CO<sub>2</sub> and  
86 mineral/water interfacial tensions as a function of pressure, temperature, salinity and mineral  
87 type. Essentially, three important issues are addressed in this work: 1) Computation of surface  
88 energy of solid/CO<sub>2</sub> and solid/brine as a function of pressure, temperature and salinity, 2) How  
89 these computed interfacial tensions explain the dependence of wettability on pressure,  
90 temperature and salinity and 3) To answer a very important question, i.e. why different minerals  
91 exhibit different wettability at the same operating conditions.

92 In this context, we used advancing and receding contact angle ( $\theta_a$  and  $\theta_r$  respectively) data for  
93 CO<sub>2</sub>/brine systems for quartz (from Al-Yaseri et al., 2016a), water-wet mica (from Arif et al.,  
94 2016a; and the mica chosen is muscovite mica), oil-wet mica (from Arif et al., 2016b) and coal  
95 (from Arif et al., 2016c) at a wide range of operating conditions and computed mineral/CO<sub>2</sub>  
96 and mineral/water interfacial tensions and analysed the associated trends. Our results depict  
97 that mineral/CO<sub>2</sub> interfacial tension decreased with pressure and increased with temperature  
98 for all minerals. However, mineral/water interfacial tension decreased with temperature for  
99 mica and coals but increased with temperature for quartz. The computed data in this paper can  
100 also be used to estimate contact angle from Young's equation at any pressure, temperature and

101 salinity using known values of surface energies. Finally, we conclude that the quantification of  
 102 surface energies is not only helpful in understanding the CO<sub>2</sub>/solid interactions but also  
 103 adequately explain the factors influencing wettability and thus considerably improve the  
 104 understanding of geological storage processes and provide independent estimates for surface  
 105 energies for various other engineering applications.

106  
 107

## 108 **2. Methodology**

109

110 We used the equation of state approach by Neumann (Neumann et al., 1974) to compute  
 111 mineral/CO<sub>2</sub> and mineral/water surface energies for a wide range of operating conditions for  
 112 quartz, water-wet mica, oil-wet mica, and coals of high, medium and low ranks. Following  
 113 sections describe the methodology in detail.

114

### 115 **2.1. Contact angle data**

116 We selected the water advancing and receding contact angle ( $\theta_a$  and  $\theta_r$ ) data from our previous  
 117 publications (quartz: from Al-Yaseri et al., 2016a, water-wet mica from Arif et al., 2016a, and  
 118 oil-wet mica from Arif et al., 2016b; high, medium and low rank coals: from Arif et al., 2016c;  
 119 Table 1). Surface energy calculations require equilibrium contact angles (see detail in section  
 120 2.2 below); these have been computed from Tadmor's empirical method (Tadmor, 2004, Table  
 121 2). Tadmor's correlation allows the calculation of equilibrium contact angles using the  
 122 corresponding values of advancing and receding contact angles. The equations are as follows:

123

$$124 \quad \theta_e = \arccos\left(\frac{\Gamma_A \cos \theta_A + \Gamma_R \cos \theta_R}{\Gamma_A + \Gamma_R}\right) \quad (2)$$

125 In equation (2),  $\theta_e$  is the equilibrium contact angle while  $\theta_A$  and  $\theta_R$  are the advancing and  
 126 receding contact angles respectively, whereas,  $\Gamma_R$  and  $\Gamma_A$  are defined as follows:

$$127 \quad \Gamma_R = \left(\frac{\sin^3 \theta_R}{2 - 3 \cos \theta_R + \cos^3 \theta_R}\right)^{1/3} \quad (3)$$

$$128 \quad \Gamma_A = \left(\frac{\sin^3 \theta_A}{2 - 3 \cos \theta_A + \cos^3 \theta_A}\right)^{1/3} \quad (4)$$

129

130 Neumann et al.'s equation of state approach also requires CO<sub>2</sub>/water interfacial tension data  
 131 which was taken from Sarmadivaleh et al. (2015) and CO<sub>2</sub>/brine interfacial tension was taken  
 132 from Arif et al. (2016a), Table 3.

133

134

135 **Table 1:** Contact angle data for CO<sub>2</sub>-deionized (DI) water systems for minerals investigated in  
 136 this study.

137

Temperature (K)	Pressure (MPa)	Quartz		Water-wet mica		Oil-wet mica		High rank coal		Medium rank coal		Low rank coal	
		$\theta_a$	$\theta_r$	$\theta_a$	$\theta_r$	$\theta_a$	$\theta_r$	$\theta_a$	$\theta_r$	$\theta_a$	$\theta_r$	$\theta_a$	$\theta_r$
		(°)	(°)	(°)	(°)	(°)	(°)	(°)	(°)	(°)	(°)	(°)	(°)
308*	0.1	0	0	10	5	90	65	37	30	32	25	43	32
	5	15	11	33	25	125	107	94	80	77	63	75	60
	10	23	17	55	50	148	128	140	126	127	115	103	87
	15	30	20	71	63	170	159	146	134	128	118	112	96
	20	37	23	80	72	172	160	151	139	137	121	122	110
323	0.1	0	0	4	0	74	64	51	45	28	22	38	27
	5	19	13	30	24	118	102	89	79	69	49	50	42
	10	30	25	48	40	143	125	129	114	108	98	94	78
	15	38	28	59	54	170	157	136	123	114	102	102	91
	20	42	35	70	62	170	158	141	129	122	112	116	107
343	0.1	0	0	0	0	73	65	58	53	18	12	27	18
	5	22	19	27	22	99	82	86	74	48	33	45	36
	10	42	30	43	36	108	91	109	97	95	85	92	77
	15	45	38	52	48	128	110	119	111	102	89	102	87
	20	50	42	62	53	156	134	125	114	113	95	110	97

138 \*contact angles are interpolated at 308 K for quartz

139

140

141 **Table 2:** Equilibrium contact angles for all minerals calculated using Tadmor's correlation.

Temperature (K)	Pressure (MPa)	Equilibrium contact angle $\theta_e$ (°)					
		Quartz	Water-wet mica	Oil-wet mica	High rank coal	Medium rank coal	Low rank coal
308	0.1	0	6	74.1	33.3	28.2	36.9
	5	12.9	28.7	112.8	85.8	69	66.4
	10	19.8	52.4	131.8	130	119	93.2

	15	24.2	66.7	159.9	137	122	102
	20	29	75.7	160.5	142	126	115
323	0.1	0	2	68.49	47.8	24.8	31.9
	5	15.7	26.8	107.7	83.4	57.1	45.7
	10	27.4	43.7	129.3	119	102	84.4
	15	32.5	56.4	157.8	127	107	95.6
	20	38.3	65.7	158.8	133	116	111
343	0.1	0	0.5	68.67	55.4	14.7	22
	5	20.4	24.3	88.62	79.2	39.4	40.1
	10	35.3	39.3	97.35	102	89.3	83.1
	15	41.3	49.9	115.6	114	94.3	92.9
	20	45.7	57.1	136.6	118	101	102

142

143

144 **Table 3:** CO<sub>2</sub>/DI-water and CO<sub>2</sub>/brine interfacial tension data used.

145

Temperature (K)	Pressure (MPa)	CO <sub>2</sub> /DI-water IFT <sup>a</sup> (mN/m)	CO <sub>2</sub> /brine* IFT <sup>b</sup> (mN/m)
308	0.1	75.8	72.9
	5	40.2	50.1
	10	28.4	38.2
	15	22.7	33.9
	20	21.0	32.3
323	0.1	73.1	72.0
	5	49	55.3
	10	35.5	42.6
	15	29	38.7
	20	26	36.0
343	0.1	65	69.2
	5	52.18	57.7
	10	43	44.8
	15	34.5	39.7
	20	27	37.7

146

147 <sup>a</sup> experimental data from Sarmadivaleh et al. (2015), values interpolated at 308 K and 323 K

148 <sup>b</sup> experimental data from Arif et al. (2016a)

149 \*20wt% NaCl in DI water

150

151

152

153

## 154 **2.2. Surface free energy computation**

155 The surface free energy of solids has been investigated by a growing number of studies (e.g.  
156 Ameri et al., 2013; Dickson et al., 2006; Kwok and Neumann, 2000; Zenkiewicz, 2007) as it  
157 is of great practical significance for many engineering applications including catalysis,  
158 coatings, flotation, printing and polymer sciences (Zenkiewicz, 2007). The most common  
159 approaches include the Zisman method (Fox and Zisman, 1952), the Fowkes method (Fowkes,  
160 1964), the geometric-mean approach (Owens and Wendt, 1969), the harmonic-mean approach  
161 (Wu, 1971), the equation of state approach or Neumann's method (Neumann et al., 1974) and  
162 the acid-base approach or van Oss-Good method (van Oss et al., 1986). We chose Neumann's  
163 equation of state method because of convenience in its application as it requires the knowledge  
164 of experimental contact angle,  $\theta$ , and CO<sub>2</sub>/water interfacial tension ( $\gamma_{cw}$ ) data for which reliable  
165 data is available.

166

167 Thermodynamically, solid/CO<sub>2</sub>, solid/water and CO<sub>2</sub>/water interfacial tensions ( $\gamma_{sc}$ ,  $\gamma_{sw}$   
168 and  $\gamma_{cw}$ ) are interrelated by an equation of state (Neumann et al., 1974), such that:

169

$$170 \quad \gamma_{sw} = f(\gamma_{sc}, \gamma_{cw}) \quad (5)$$

171

172 Neumann et al. (1974) used the hypothesis that the free energy of adhesion per unit area of a  
173 solid-liquid pair is equal to the work required to separate a unit area of solid-liquid interface  
174 and that free adhesion energy was proposed to be equal to the geometric mean of the solid  
175 cohesion work and the liquid cohesion work. These geometric means were combined so that  
176 equation (6) resulted (for a complete derivation the reader is referred to Ameri et al., 2013).

177

$$178 \quad \gamma_{sw} = \gamma_{sc} + \gamma_{cw} - 2\sqrt{\gamma_{cw}\gamma_{sc}}[1 - \beta(\gamma_{cw} - \gamma_{sc})^2] \quad (6)$$

179

180 The equation (7) below was then derived by Ameri et al., (2013) to find an expression for  $\gamma_{sc}$   
181 instead of  $\gamma_{sw}$  as shown:

182

183

$$\gamma_{sc} = \gamma_{sw} + \gamma_{cw} - 2\sqrt{\gamma_{cw}\gamma_{sw}}[1 - \beta(\gamma_{cw} - \gamma_{sw})^2] \quad (7)$$

184

185 ‘ $\beta$ ’ is a constant which is related to the fit of the original experimental data (Neumann et al.,  
186 1974) to the model and in the present case it can be determined by non-linear regression of  
187 contact angle ( $\theta$ ) and CO<sub>2</sub>/water interfacial tension data ( $\gamma_{cw}$ ) as further explained below.

188

189 Combining Eq. (1) and (7), one obtains:

190

$$\cos \theta_e = 1 - 2 \sqrt{\frac{\gamma_{sw}}{\gamma_{cw}}} [1 - \beta(\gamma_{cw} - \gamma_{sw})^2] \quad (8)$$

191 Ameri et al., (2013) applied equation (7) and (8) to determine solid/CO<sub>2</sub> interfacial tension of  
192 oil-wet Bentheimer sandstone as a function of pressure and they reported the corresponding  
193 values of solid/liquid interfacial tension derived by non-linear regression. To account for a  
194 systematic evaluation of wettability dependence on pressure, temperature and salinity, we  
195 express equations (7) and (8) to clearly demonstrate that these are functions of pressure,  
196 temperature and salinity:

197

198

$$\gamma_{sc(P,T,S)} = \gamma_{sw(T,S)} + \gamma_{cw(P,T,S)} - 2\sqrt{\gamma_{cw(P,T,S)}\gamma_{sw(T,S)}} [1 - \beta(\gamma_{cw(P,T,S)} - \gamma_{sw(T,S)})^2] \quad (9)$$

199

200

201

$$\cos \theta_{e(P,T,S)} = 1 - 2 \sqrt{\frac{\gamma_{sw(T,S)}}{\gamma_{cw(P,T,S)}}} [1 - \beta(\gamma_{cw(P,T,S)} - \gamma_{sw(T,S)})^2] \quad (10)$$

202

203 The scripts P, T and S refer to pressure, temperature and salinity, respectively, and are added  
204 to the interfacial energy terms to elucidate their dependence on them. It is notable that  $\gamma_{sw}$  is  
205 dependent on temperature and salinity but not on pressure (Ameri et al., 2013; Neumann et al.,  
206 1974). This is the basic assumption of the Neumann’s equation of state.

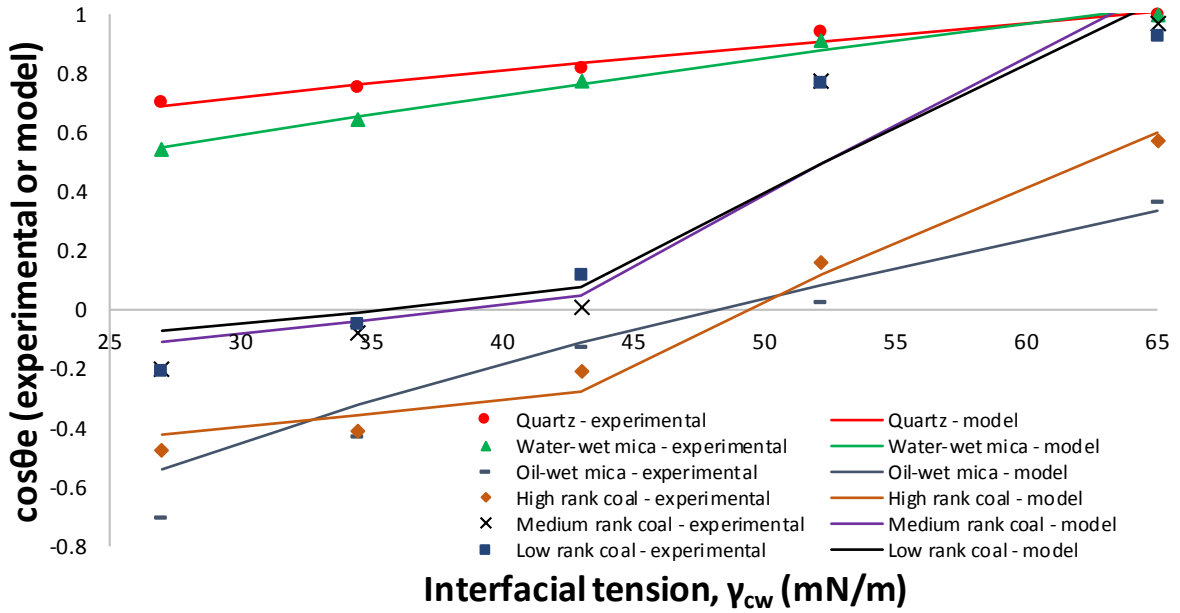


207 Our computations begin with input data acquisition which includes a) advancing and receding  
208 contact angle data for quartz (Al-Yaseri et al., 2016a), water-wet mica (Arif et al., 2016a), oil-  
209 wet mica (Arif et al., 2016b) and coals of high medium and low ranks (Arif et al., 2016c) listed  
210 in Table 1, and b) CO<sub>2</sub>/water interfacial data (Sarmadivaleh et al., 2015), listed in Table 3.  
211 Then,  $\cos\theta_e$  (cosine of the equilibrium contact angle) is calculated using advancing and  
212 receding contact angle data for all cases analysed (results in Table 2). In the next step,  $\gamma_{sw(T)}$   
213 and the constant ‘ $\beta$ ’ are determined by least squares fitting of the  $\cos\theta_e$  and  $\gamma_{cw}$  data. To  
214 accomplish this,  $\cos\theta_e$  is first calculated by using equation (10) for any trial values of  $\gamma_{sw(T)}$   
215 and ‘ $\beta$ ’ and is plotted against  $\gamma_{cw}$  (this data is referred as model data). Moreover, the  
216 experimental  $\cos\theta_e$  (Table 2) is also plotted against  $\gamma_{cw}$  (such a plot is shown in Figure 1 for all  
217 minerals analysed at 343 K), the regression analysis of these data-sets yield final values of  
218  $\gamma_{sw(T)}$  and ‘ $\beta$ ’ corresponding to the best-fit (note: such plots are created at all three analysis  
219 temperatures and for all minerals, and directly provide values of  $\gamma_{sw(T)}$  as a function of  
220 temperature). Finally, using these calculated values, solid/CO<sub>2</sub> interfacial tension is computed  
221 using equation (9) as a function of pressure, temperature, salinity and type of the mineral.

222

### 223 **2.3. Regression fit of data**

224 As a first step,  $\cos\theta_e$  (experimental) is plotted against  $\gamma_{cw}$  and on the same plot  $\cos\theta_e$  (calculated  
225 using equation 10 for arbitrary values of  $\gamma_{sw}$  and ‘ $\beta$ ’) is also plotted against  $\gamma_{cw}$ . Such plots are  
226 constructed corresponding for each temperature and for all five cases analysed. An example is  
227 shown in Figure 1, where, for simplicity, only a temperature of 343 K is shown, but for all five  
228 minerals investigated. The model and experimental data are in a good agreement, however the  
229 model predictions are sensitive to CO<sub>2</sub>/water interfacial tension values and thus reliable  
230 CO<sub>2</sub>/interfacial tension input is required for reliable modelling of solid/fluid interfacial  
231 tensions.



232

233

234 **Figure 1:** Regression fit of experimental and model data for all minerals investigated at 343  
 235 K.

236

237 The  $R^2$ -values, fitting parameters ' $\beta$ ' and  $\gamma_{sw}$  were computed for each case from the regression  
 238 fits and the results are tabulated in Table 4. The standard deviations in experimental contact  
 239 angle and interfacial tension data used were  $\pm 3^\circ$  and  $\pm 3$  mN/m respectively.

240

241 **Table 4:** Results obtained from regression fit of the experimental and model data.

Case	Temperature (K)	$R^2$	$\beta$	$\gamma_{sw}$ (mN/m)
Quartz	308	0.898	0.000205	0.058
	323	0.943	0.000219	0.284
	343	0.988	0.0002524	0.952
Water-wet mica	308	0.899	0.00022	2.178
	323	0.935	0.00023	2.048
	343	0.992	0.00027	1.98
Oil-wet mica	308	0.9857	0.000166	20.19
	323	0.988	0.00022	25.47
	343	0.92	0.000145	16.53
High rank coal	308	0.9778	0.00033	20.25
	323	0.952	0.00028	19.23

	343	0.944	0.00021	15.37
Medium rank coal	308	0.994	0.00031	16.17
	323	0.974	0.0003	13.87
	343	0.93	0.00034	10.81
Low rank coal	308	0.989	0.00022	11.22
	323	0.954	0.0003	10.38
	343	0.946	0.00032	10.12

242

243

244

245

### 246 **3. Results and discussion**

247

248 We computed solid/CO<sub>2</sub> interfacial tension as a function of pressure, temperature and salinity  
 249 and solid/water interfacial tension as a function of temperature and salinity via Neumann's  
 250 equation of state (Neumann et al., 1974) for quartz, mica and coals using experimental contact  
 251 angle data and CO<sub>2</sub>/brine interfacial tension data. The results broaden the understanding of  
 252 rock/fluid interaction properties. Specifically, the results of this study allow the understanding  
 253 of the influence of surface energy on rock wettability as a function of pressure, temperature,  
 254 salinity, and type of mineral. Thus, the results contribute to a better understanding of storage  
 255 mechanisms which ensure containment security (Iglauer et al., 2015b; Krevor et al., 2012;  
 256 Krevor et al., 2015).

257

258

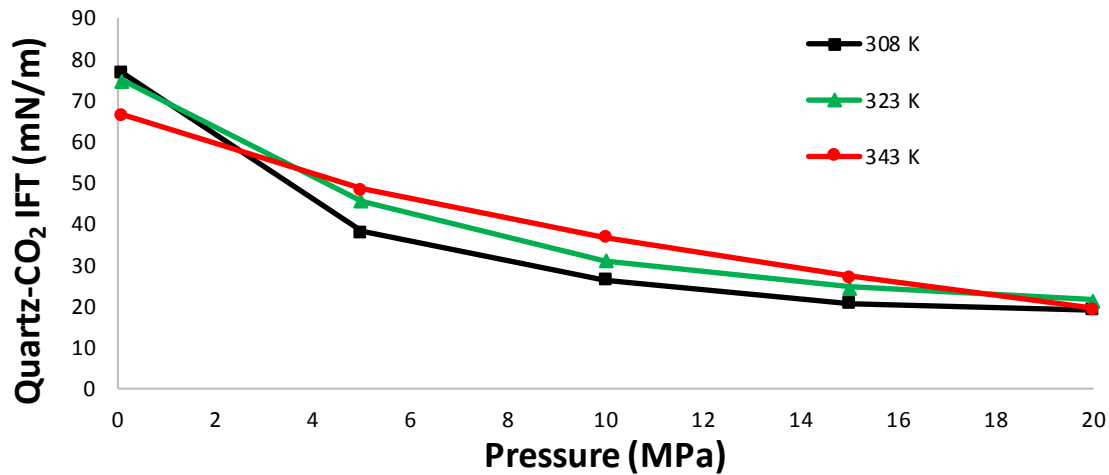
#### 259 **3.1. Effect of pressure on solid/CO<sub>2</sub> interfacial tension**

260

##### 261 *3.1.1 Case 1: quartz*

262  $\gamma_{sc}$  (solid/CO<sub>2</sub> interfacial tension) decreased with pressure at all temperatures and for all cases  
 263 analysed (Figure 2-4). As the pressure increased from 0.1 MPa to 10 MPa, quartz/CO<sub>2</sub>  
 264 interfacial tension decreased sharply from 75 mN/m to 31 mN/m at 323 K (Figure 2). However,  
 265 the decrease flattened for an additional pressure increment (from 15 MPa to 20 MPa it changed  
 266 from 24.6 mN/m to 21.6 mN/m, a reduction of only 3 mN/m). A similar trend was found at  
 267 elevated temperature, 343 K. Physically, as the pressure increases, the cohesive energy density  
 268 of CO<sub>2</sub> increases and approaches to the cohesive energy of the substrate (Dickson et al., 2006).

269 Eventually, the interactions between solid and CO<sub>2</sub> become more favourable and as a result  
 270 quartz/CO<sub>2</sub> interfacial energy decreases with pressure. Note that at pressure = 0.1 MPa, a switch  
 271 in temperature occurs due to a switch in CO<sub>2</sub>/water interfacial tensions; Table 3 (Arif et al.,  
 272 2016a).  
 273



274  
 275 **Figure 2:** Quartz/CO<sub>2</sub> interfacial tension as a function of pressure and temperature.

276  
 277 A few studies report surface free energies of quartz at ambient conditions. Janczuk and  
 278 Zdziennicka, (1994) calculated the surface energy of quartz at ambient conditions against air  
 279 using the van Oss-Good method (van Oss et al., 1986) and the values ranged from 57 mN/m to  
 280 126 mN/m, consistent with our value (~74 mN/m) estimated for a similar condition (0.1 MPa  
 281 and 308 K).

282  
 283 Dickson et al. (2006) is the only major study which computed surface energies as a function of  
 284 pressure for silica (glass)/CO<sub>2</sub> systems and found that for a partially methylated glass surface  
 285 (63% of the surface was covered by methyl groups, the remaining 37% by SiOH groups)  
 286 surface solid/CO<sub>2</sub> interfacial tension decreased with pressure. The values reported were 38  
 287 mN/m at a CO<sub>2</sub> activity of 0 (equivalent to a pressure of 0.1 MPa) and reduced to ~10 mN/m  
 288 at a CO<sub>2</sub> activity of 1.4 (equivalent to 20 MPa) at 296 K. The decrease in quartz/CO<sub>2</sub> interfacial  
 289 tension with pressure is thus consistent with Dickson et al. (2006), however, the difference in  
 290 values is due to the fact that the surface they used had only 37% silanol group coverage (while  
 291 in our case it is 100%, i.e. pure quartz). Furthermore, Dickson et al. (2006) reported solid/CO<sub>2</sub>  
 292 interfacial tension for a 12% SiOH surface (now 88% of the surface was methylated), for which  
 293 lower  $\gamma_{sc}$  values were reported (20 mN/m at 0.1 MPa and ~0 mN/m at 20 MPa) which is due to

294 the higher hydrophobicity of the 12% SiOH surface (when compared with the 37% SiOH  
295 surface). Due to the limited number of silanol groups available, only a minimal amount of CO<sub>2</sub>  
296 is expected to cap these hydrophilic sites, thus  $\gamma_{sc}$  values were lower for lower silanol coverage  
297 (e.g. for our case  $\gamma_{sc} = 20$  mN/m at 20 MPa, and for Dickson et al.  $\gamma_{sc} = 10$  mN/m for 37% SiOH  
298 surface, and  $\sim 0$  mN/m for 12% SiOH surface).

299 The higher values of quartz/CO<sub>2</sub> interfacial tensions as compared to mica (see below) at a given  
300 pressure and temperature imply that quartz is more hydrophobic in nature.

301

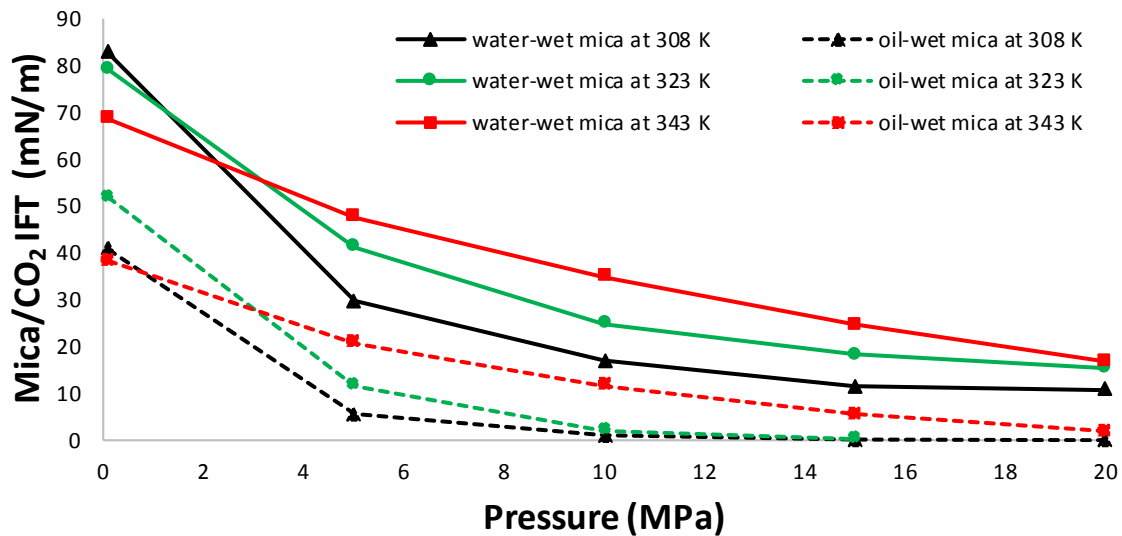
### 302 3.1.2 Case 2: Mica

303 Two mica surfaces were analysed: a) naturally water-wet mica (Arif et al., 2016a) and b) oil-  
304 wet mica (treated with silane to achieve oil-wet conditions, ambient air/water contact angle =  
305 120°, Arif et al., 2016b). The results indicate that, likewise quartz, mica/CO<sub>2</sub> interfacial tension  
306 decreased with pressure for both water-wet and oil-wet mica surfaces (Figure 3). When  
307 pressure increased from 0.1 MPa to 5 MPa, mica/CO<sub>2</sub> interfacial tension decreased sharply  
308 from 78 mN/m to 41 mN/m, for water-mica. Gradually, the decrease flattened out with further  
309 increase in pressure (24 mN/m at 10 MPa and 16 mN/m at 20 MPa). Similar trends were found  
310 for oil-wet mica surface. However, at any given pressure, the mica/CO<sub>2</sub> interfacial tension was  
311 considerably higher for water-wet mica. For example, at 10 MPa and 343 K, mica/CO<sub>2</sub>  
312 interfacial tension was 40 mN/m for water-wet mica and only 4.6 mN/m for oil-wet mica  
313 surface. This result is quite remarkable – as it demonstrates that the hydrophobic surfaces (e.g.  
314 oil-wet mica - higher water contact angles) have considerably lower solid/CO<sub>2</sub> interfacial  
315 energies in comparison to the hydrophilic surfaces (e.g. water-wet mica, lower water contact  
316 angles, and quartz, even lower contact angles than water-wet mica). The permanent oil coating  
317 on the mica (to be precise: the C12 alkyl rests chemically bonded to the surface) is responsible  
318 for the low surface energy of the oil-wet mica surface. Moreover, it can also be established that  
319 the higher the solid/vapour surface energy, the higher is the tendency of the surface to wet with  
320 water (i.e. lower contact angles, e.g. Table 1). The results are consistent with Ameri et al.  
321 (2013) who used a similar methodology and computed interfacial interaction of CO<sub>2</sub> and oil-  
322 wet Bentheimer. Their results show that at any pressure, solid/CO<sub>2</sub> interfacial tension was  
323 lower for the more oil-wet cores. For instance, at 10 MPa and 318 K, solid/CO<sub>2</sub> interfacial  
324 tensions were 20 mN/m for relatively more water-wet Bentheimer (SB-1) and 1 mN/m for oil-  
325 wet Bentheimer (SB-6, Ameri et al. 2013).

326 These results are significant for understanding the fluid flow dynamics in oil-wet and water-  
327 wet reservoir and caprocks (Iglauer et al. 2015a), and also for material design and development

328 where the physicochemical surface characteristics (e.g. surface energy) play a key role for a  
 329 wide range of operating conditions (Zenkiewicz, 2007).

330



331

332 **Figure 3:** Mica/CO<sub>2</sub> interfacial tension as function of pressure and temperature.

333

334

### 335 3.1.3 Case 3: Coals

336

337 Three coal samples [high rank (semi anthracite; from Hazelton, Pennsylvania, USA), medium  
 338 rank (medium volatile bituminous; from Morgantown, West Virginia, USA), and low rank  
 339 (lignite; from North Dakota, USA)] were analysed for surface energy calculations. Advancing  
 340 and receding contact angle data for the three coals is taken from our previous work (Arif et al.,  
 341 2016c, Table 1). The detailed description of the properties of these coal sample can be found  
 342 elsewhere (Arif et al., 2016c), however the mineral identified by XRD in the three samples  
 343 revealed that the major minerals present were illite, quartz and kaolinite. We note that the  
 344 measured contact angles may slightly vary with the mineralogy of coal; thus the results  
 345 reported here must be accompanied with the mineralogy of the specific sample under  
 346 investigation. Results showed that coal/CO<sub>2</sub> interfacial tension also decreased with pressure  
 347 irrespective of the coal rank (Figure 4). For all coals, the coal/CO<sub>2</sub> interfacial tension decreased  
 348 sharply for the pressure interval 0.1 MPa-5 MPa, e.g. for high rank coal, at 308 K, coal/CO<sub>2</sub>  
 349 interfacial tension decreased from 84 mN/m to ~12 mN/m when pressure increased from 0.1  
 350 MPa to 5 MPa. However,  $\gamma_{sc}$  turned almost constant for the pressure interval 10 MPa – 20 MPa  
 351 (Figure 4). Moreover, at a given pressure, the low rank coals exhibited the highest coal/CO<sub>2</sub>

352 interfacial tension values, while the high rank coal had the lowest coal/CO<sub>2</sub> interfacial tension,  
353 e.g. at 10 MPa and 323 K, coal/CO<sub>2</sub> interfacial tensions were 4.7 mN/m, 7.4 mN/m, and 10.2  
354 mN/m for high, medium and low rank coals, respectively. At ambient conditions, Staszczuk  
355 (1989) determined surface free energy of coal, and found that the dispersion component was  
356 45 mN/m and polar component measured 13 mN/m, thus a total surface energy of 58 mN/m  
357 comparable to our results ~ 70 mN/m for low rank coal at 308 K and 0.1 MPa.

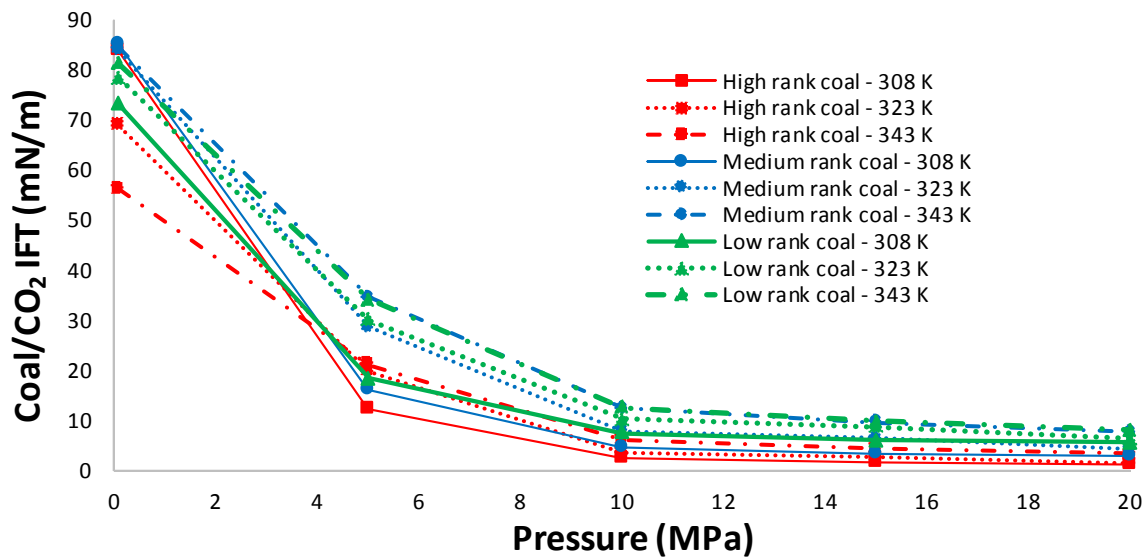
358

359 In order to explain the variation of coal/CO<sub>2</sub> interfacial tension with coal rank, we conducted  
360 FTIR (Fourier Transformed infrared) spectroscopy measurements on the coal samples (Figure  
361 5). Low rank coal demonstrated the largest peak beginning at about 2800 cm<sup>-1</sup> and ending at  
362 3800 cm<sup>-1</sup> which is attributed to the O-H and N-H stretch vibrations (Socrates, 2004) while  
363 high rank coal exhibited negligible O-H and N-H stretch vibrations at 3800 cm<sup>-1</sup>. The  
364 abundance of these hydrophilic sites in low rank coal and absence of these sites in high rank  
365 coal is responsible for higher coal/CO<sub>2</sub> interfacial tensions for low rank coal and low coal/CO<sub>2</sub>  
366 interfacial tension for high rank coal. The band at ~2900 cm<sup>-1</sup> observed for low and medium  
367 rank coal is due to the presence of aliphatic C-H stretching vibrations (Wu et al., 2014);  
368 however, its absence in high rank coal is unusual and is perhaps due to C-H stretching where  
369 the carbon is in a C=C bond. The rough part of the spectra for 2000-2400 cm<sup>-1</sup> should be  
370 ignored as this is where the ATR crystal is absorbing itself (diamond) and the bands don't  
371 always perfectly cancel out.

372 Moreover, the sharp band observed at 1500-1800 cm<sup>-1</sup> for low and medium rank coal is  
373 attributed to aromatic ring vibrations, which are enhanced by oxygen groups (Sarwar et al.,  
374 2012). The corresponding shoulder peaks at 1600 cm<sup>-1</sup> for low and medium rank coals is  
375 attributed to C=O stretching vibrations and these represent all C=O functionalities, e.g.  
376 carboxylic acids or phenolic esters (Manoj et al., 2009). Furthermore, low and medium rank  
377 coal (medium volatile bituminous) exhibited significantly stronger bands (in comparison to  
378 high rank coal) at wave numbers from 600-800 cm<sup>-1</sup> and 1000-1100 cm<sup>-1</sup> indicating presence  
379 of more C-S stretching vibrations and C-H out of plane bending.

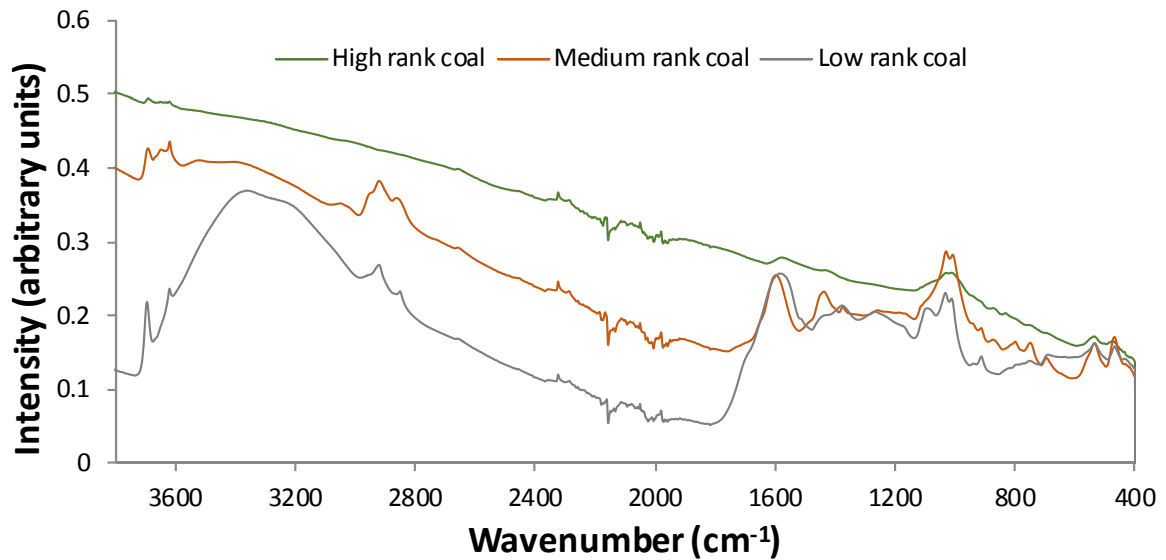
380 Thus, low rank coal has more polar functional groups on the surface than medium rank coal,  
381 and thus fewer attractive forces between the more polar surface and the non-polar (here in the  
382 sense of no external dipole moment) CO<sub>2</sub> generated, which lead to the higher coal/CO<sub>2</sub>  
383 interfacial tension for low rank coal at any pressure as compared to medium and high rank coals  
384 (Figure 4).

385  
386  
387



388  
389  
390

**Figure 4:** Coal/CO<sub>2</sub> interfacial tension as a function of pressure, temperature and coal rank.



391  
392

**Figure 5.** ATR-Infrared spectra for low, medium and high rank coals.

394

395 Note that high surface energy corresponds to strong cohesive forces and higher boiling points  
396 (Tripp and Combes, 1998). Moreover, high energy surfaces tend to reduce energy by  
397 adsorption of contaminants from the environment (Tripp and Combes, 1998).

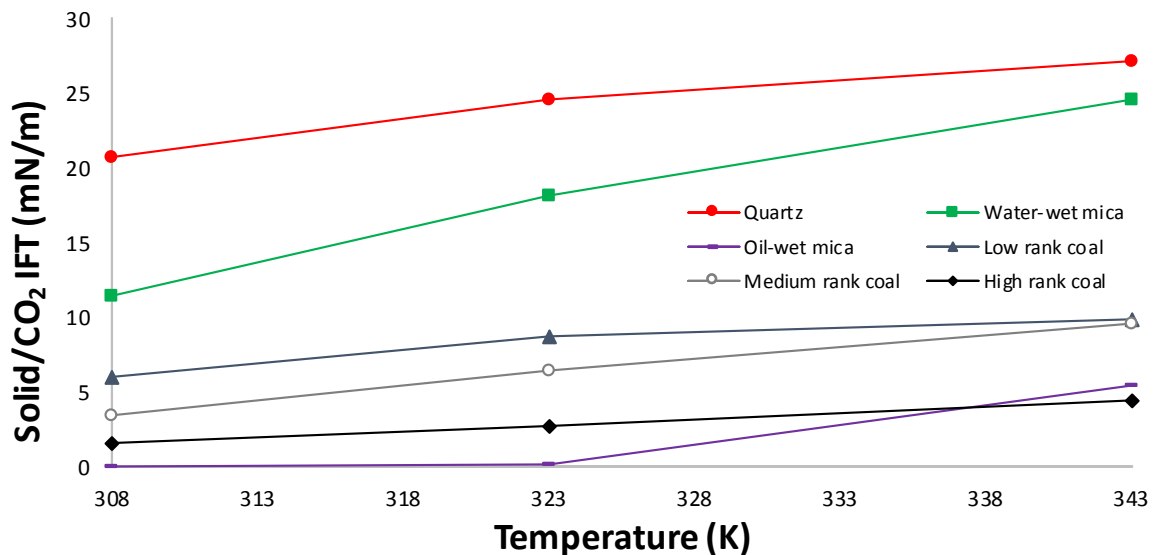


398

### 399 3.2. Effect of temperature on solid/CO<sub>2</sub> interfacial tension

400

401 For all cases analysed, the solid/CO<sub>2</sub> interfacial tension increased with temperature (Figures 2-  
402 4). For simplicity, a plot of solid/CO<sub>2</sub> interfacial tensions for the temperature range 308-343 K  
403 at 15 MPa is presented in Figure 6.



404

405

406 **Figure 6:** Solid/CO<sub>2</sub> interfacial tension as a function of temperature at 15 MPa for various  
407 substrates.

408

409 Quartz/CO<sub>2</sub> interfacial tension increased from 21 mN/m to 27 mN/m when temperature  
410 increased from 308 K to 343 K (Figure 6). Moreover, solid/CO<sub>2</sub> interfacial tension was highest  
411 for quartz, and lowest for oil-wet mica at any pressure and temperature.

412 Mica/CO<sub>2</sub> interfacial tension also followed a similar trend. For water-wet mica, mica/CO<sub>2</sub>  
413 interfacial tension increased from 11.5 mN/m to 24 mN/m when temperature increased from  
414 308 K to 343 K, while for the same temperature interval, for oil-wet mica, mica/CO<sub>2</sub> interfacial  
415 tension increased from ~ 0 mN/m to 5 mN/m. Moreover, oil-wet mica demonstrated the lowest  
416 values of mica/CO<sub>2</sub> interfacial tension out of all cases at any pressure and temperature which  
417 is again attributed to reduced number of polar sites on oil-wet mica surface.

418 Coal/CO<sub>2</sub> interfacial tension also decreased with temperature, (Figure 6). For instance, for low  
419 rank coal, coal/CO<sub>2</sub> interfacial tension increased from 6 mN/m to ~ 9.5 mN/m when  
420 temperature increased from 308 K to 343 K. Moreover, high rank coal had the lowest coal/CO<sub>2</sub>  
421 interfacial tension at any temperature which is due to the lower concentration of polar surface

422 groups on the high rank coal (see above and Figure 5). Moreover, we point out that higher  
423 coal/CO<sub>2</sub> interfacial tensions reduces CO<sub>2</sub>-adsorption in coals (because CO<sub>2</sub>-adsorption in  
424 coals also decreases with temperature, Bustin and Clarkson, 1998).

425 For all cases analysed, the increase in  $\gamma_{sc}$  with temperature is attributed to a decrease in cohesive  
426 energy density of CO<sub>2</sub> with temperature (Barton, 1991) while the cohesive energy density of  
427 the solid is expected to stay approximately constant with temperature (Kittel, 2005), which  
428 leads to an increase in the difference of solid/CO<sub>2</sub> cohesive energies with temperature.  
429 Consequently, the interactions between solid and CO<sub>2</sub> become less favourable, thus  $\gamma_{sc}$   
430 increases with temperature which promotes water-wetting of the surface. Moreover, reduction  
431 in CO<sub>2</sub> density with temperature leads to fewer van der Waals interactions which leads to an  
432 increase in  $\gamma_{sc}$  with temperature.

433

434

### 435 *3.3. Effect of temperature on solid/water interfacial tension*

436

437 Solid/water interfacial tension is directly computed from the regression fit of the experimental  
438 and model data and the results are shown in Table 4. For all cases, the solid/water interfacial  
439 tension decreased with increasing temperature except for quartz, for which it increased with  
440 temperature. However, the absolute quartz  $\gamma_{sw}$  was very low and so were the changes in  $\gamma_{sw}$ .  
441 When temperature increased from 308 K-343 K the quartz/water interfacial tension increased  
442 from 0.058 mN/m to 0.952 mN/m. Recently, Shojai Kaveh et al. (2016) calculated interfacial  
443 energy of shale/water systems and found that the values of shale/water interfacial tension was  
444 also quite low (0.58 mN/m at 318 K), consistent with our results. The increase in quartz/water  
445 interfacial tension with temperature is due to desorption of water molecules from the surface  
446 (Janczuk and Zdziennicka, 1994).

447 For mica, at any temperature, the solid/water interfacial tensions were notably higher for oil-  
448 wet mica and lower for water-wet mica (e.g.  $\gamma_{sw} = \sim 25$  mN/m for oil-wet mica (21% carbon  
449 coverage, Arif et al., 2016b), and  $\sim 2$  mN/m for water-wet mica (0% carbon coverage, unaltered  
450 surface, Arif et al., 2016b) at the same temperature, 323 K and pressure, 10 MPa). The larger  
451 solid/liquid interfacial tension values for the more hydrophobic surface is consistent with  
452 Dickson et al. (2006) who reported that the glass surface with higher silanol coverage had lower  
453 solid/liquid interfacial tensions (note: a higher concentration of surface silanol groups creates  
454 a more hydrophilic surface (Chen et al., 2015; McCaughan et al., 2013). Specifically, the  
455 calculated  $\gamma_{sw}$  values for the 37% SiOH and 12% SiOH surfaces were 13.2 and 29.2 mN/m

456 respectively (Dickson et al., 2006), quite comparable to our results for the oil-wet mica  
457 surfaces. The results are also consistent with Ameri et al. (2013) who reported that  $\gamma_{sw}$  was  
458 significantly lower for water-wet sandstones ( $\gamma_{sw} = 2.88$  mN/m) as compared to oil-wet  
459 sandstones ( $\gamma_{sw} = 27.22$  mN/m).

460 Coal surfaces also exhibited similar trends, i.e.  $\gamma_{sw}$  decreased with increasing temperature, and  
461 the values of coal/water interfacial tension were higher for high rank coal and lower for low  
462 rank coal (e.g. at 323 K,  $\gamma_{sw}$  was 19.23 mN/m for high rank coal, 13.87 mN/m for medium  
463 rank coal and 10.38 mN/m for low rank coals, Table 4). This effect is attributed to an abundance  
464 of hydrophilic sites (OH functional groups, typically silanol) in low rank coal and absence of  
465 hydrophilic sites in high rank coal. Essentially, presence of silanol sites leads to favourable  
466 interactions between coal surface and water, thereby resulting in a reduction of  $\gamma_{sw}$  for low  
467 rank coal.

468 Further, we point out that the proposed methodology assumes that  $\gamma_{sw}$  is constant versus  
469 pressure. In reality, however, the solid/water interactions are expected to change due to increase  
470 in solubility of CO<sub>2</sub> in water with pressure (El-Maghraby et al. 2012), and associated lower pH  
471 values (Schaeff and McGrail, 2004), which leads to increased protonation of the silanol surface  
472 groups (Brown et al., 2012).

473

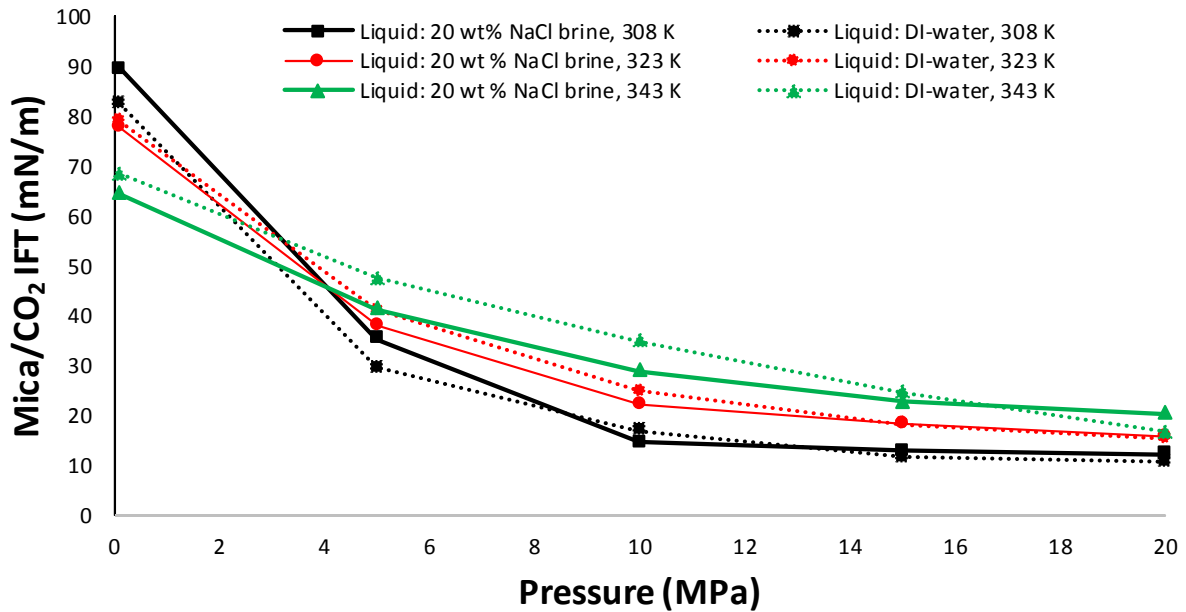
#### 474 *3.4. Effect of salinity on solid/CO<sub>2</sub> interfacial tension*

475

476 We compared solid/CO<sub>2</sub> interfacial tension (as function of pressure and temperature) for 20  
477 wt% NaCl brine in mica/CO<sub>2</sub> systems and compared it with that of mica/water systems. The  
478 results showed that the mica/CO<sub>2</sub> interfacial tension for DI-water at a particular pressure and  
479 temperature is quite similar to the mica/CO<sub>2</sub> interfacial tension for 20 wt % NaCl brine case  
480 (Figure 7). For instance, at 323 K, and 10 MPa, the mica/CO<sub>2</sub> interfacial tensions were 22.4  
481 mN/m for liquid comprising of 20 wt% NaCl brine, and 24.8 mN/m for DI-water, thus a  
482 difference of only 2.4 mN/m (Figure 7). Moreover, at the same temperature but at 15 MPa,  
483 mica/CO<sub>2</sub> interfacial tension for two different liquids (DI water and 20 wt % NaCl brine) is the  
484 same (~18.5 mN/m, Figure 7). In summary, the R<sup>2</sup>-values for the correlation between mica/CO<sub>2</sub>  
485 interfacial tensions for the two liquids were 0.997, 0.998 and 0.985 at 308 K, 323 K and 343  
486 K, respectively, indicating a strong correlation. This implies that solid/CO<sub>2</sub> interfacial tension  
487 is not much changed by altering the type of the liquid in the same system. We point out that

488 this result verifies this methodology and our predictions (of mineral/CO<sub>2</sub> and mineral/water  
 489 interfacial tensions) to some extent.

490



491

492 **Figure 7:** Mica/CO<sub>2</sub> interfacial tension as a function of pressure and temperature for two  
 493 different liquids (DI-water and 20 wt% NaCl brine)

494

495

### 496 3.5. Effect of salinity on solid/water interfacial tension

497 To analyse the effect of salinity on the solid-water interfacial energies, we compared  $\gamma_{sw}$  results  
 498 for DI water (see above) with that of 20 wt% NaCl brine. The  $\beta$  values from the non-linear  
 499 regression fit of cosine of the equilibrium contact angle data were 0.000267, 0.000284, and  
 500 0.00034 at 308 K, 323 K and 343 K, respectively. The Pearson coefficients were 0.846, 0.921  
 501 and 0.941, indicating good fits. The mica/brine (20wt% NaCl) interfacial tensions were 10.5  
 502 mN/m, 6.27 mN/m and 4.4 mN/m at 308 K, 323 K and 343 K, respectively implying that  
 503 mica/brine interfacial tension decreased with temperature, consistent with the solid/DI-water  
 504 system (discussed above). However, at any given temperature, mica/brine interfacial tension  
 505 was larger than the mica/water interfacial tension. For instance, at 308 K, mica/brine (20 wt %  
 506 NaCl brine) interfacial tension was 10.5 mN/m in comparison to 2.1 mN/m for mica/DI water  
 507 at the same temperature (308 K). This result is consistent with Ameri et al. (2013) who found  
 508 that when salinity increased from 0wt% NaCl to 3.5 wt% NaCl,  $\gamma_{sw}$  increased slightly.  
 509 However, Shoaaji Kaveh et al. (2016) found a slight reduction in  $\gamma_{sw}$  with salinity. The increase

510 in solid/brine interfacial tension with salinity is related to the intermolecular forces and the zeta  
511 potential which arises due to charged species on the surface. As salinity increases, more counter  
512 ions are available to reduce the net charge and thus reduces the polarity of the surface, which  
513 again leads to a reduction in water-surface van der Waals forces. Lower van der Waals  
514 interactions result in higher interfacial tensions. Moreover, Roshan et al. (2016), recently  
515 introduced a model to describe the physical processes for wettability variation as a function of  
516 salinity in which they related electric potential at the mineral surface to the contact angle. Their  
517 results showed that as salinity increased the surface became more hydrophobic due to a  
518 decrease in the dielectric constant of liquid with salinity.

519

520

### 521 *3.6. Wettability dependence on surface energies*

522 In order to evaluate the net effect of these interfacial tensions on contact angle, the right hand  
523 side (RHS) of Young's equation (the value of  $\cos\theta$ ) was calculated for all cases analysed using  
524 the computed values of  $\gamma_{sc}$ ,  $\gamma_{sw}$  and experimental values of  $\gamma_{cw}$ . For quartz,  $\cos\theta$  decreases  
525 with pressure and temperature because quartz/ $\text{CO}_2$  interfacial tension decreases with pressure  
526 and increases with temperature, and the quartz/water interfacial tension increases with  
527 temperature. Thus the net effect of the three interfacial tension results in decrease in a  $\cos\theta$   
528 with pressure and temperature and consequently  $\theta$  increases with pressure and temperature for  
529 quartz (consistent with experimental data, Table 1). For all other cases (mica and coals),  $\cos\theta$   
530 decreases with pressure and increases with temperature because solid/ $\text{CO}_2$  interfacial tension  
531 decreases with pressure and increases with temperature and the solid/water interfacial tension  
532 also decreases with temperature (for mica and coals), thus  $\theta$  increases with pressure and  
533 decreases with temperature (consistent with experimental data, Table 1).

534 Moreover, for water-wet mica,  $\cos\theta$  stays positive for all tested pressures and temperatures,  
535 because the mica surface remains either strongly water-wet or weakly water-wet (contact angle  
536  $< 90^\circ$ , cp. Iglauer et al., 2015a, Table 1); however for the oil-wet mica surface,  $\cos\theta$  reaches  
537 negative values for a wide range of tested pressures and temperatures which indicates  $\text{CO}_2$ -wet  
538 conditions exhibited by this surface (contact angle  $> 90^\circ$ , Iglauer et al., 2015a, Table 1).  
539 Moreover,  $\theta$  increased more rapidly for oil-wet mica (as compared to water-wet mica), because  
540 of the low  $\text{CO}_2$ -solid interfacial energy, which promotes de-wetting of the surface by water  
541 (Dickson et al., 2006). Because high energy fluids (e.g. water), do not tend to spread on low-  
542 energy surfaces, the presence of a low energy  $\text{CO}_2$  layer will cause the solid/water contact angle  
543 to increase above  $90^\circ$  to increase the interfacial area between water and  $\text{CO}_2$ . Furthermore, for

544 mica and coals,  $\theta$  decreases with temperature because the net effect of solid/fluid and fluid/fluid  
545 interfacial tensions gives rise to an increase in the  $\cos\theta$  with temperature.

546 In summary, the increase in contact angle with pressure is due to a reduction in the difference  
547 of solid and CO<sub>2</sub> cohesive energies with pressure which leads to more favourable interactions  
548 between solid and CO<sub>2</sub>. Consequently,  $\gamma_{sc}$  decreases with pressure and thus promotes de-  
549 wetting of the surface (i.e. higher water contact angle).

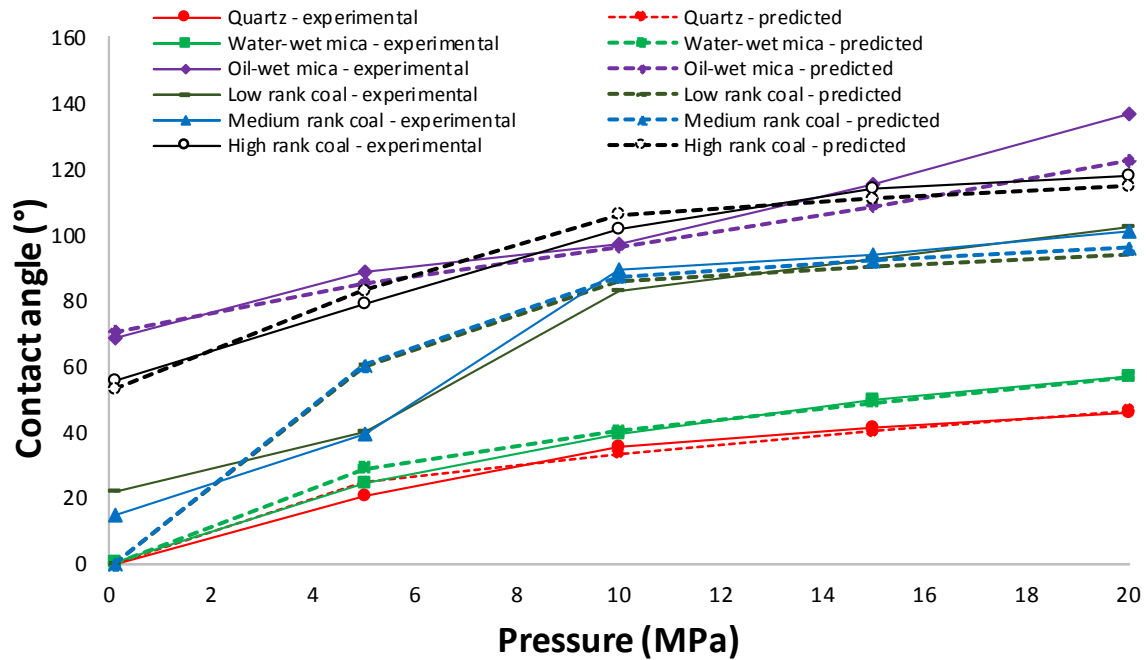
550

551

#### 552 **4. Implications**

553

554 We predicted solid/CO<sub>2</sub> and solid/water interfacial tensions for various rock forming minerals  
555 including quartz, mica and coals for a wide range of pressure and temperature conditions. The  
556 results imply that the surfaces which are more non-wetting to water exhibit lower values of  
557 solid/CO<sub>2</sub> interfacial tension than the surfaces which are more water-wet (e.g. 18 mN/m for  
558 water-wet mica in comparison to ~3mN/m for oil-wet mica at 15 MPa and 323 K). Moreover,  
559 the less water-wet surfaces have higher solid/water interfacial tensions than the water-wet  
560 surfaces (24.8 mN/m for oil-wet mica and ~2 mN/m for water-wet mica, Figure 5).  
561 Computations of these surface energies in conjunction with Young Laplace's equation enables  
562 us to predict contact angles. As an example,  $\theta$  values are predicted using Young's equation  
563 (Equation 1) using the calculated values of the interfacial tensions and the results are shown at  
564 343 K for all samples analysed (Figure 8). The results show a good match between  
565 experimental contact angle and the predicted contact angles. This implies that the methodology  
566 considered in this work to compute surface energies is correct and that the predicted solid-fluid  
567 interfacial tensions correctly reproduced experimental contact angle data.



568  
569

570 **Figure 8:** Experimental and predicted water contact angles as a function of pressure at 343 K  
571 for all substrates.

572

573 In terms of a broader interpretation, the solid/fluid interfacial tensions reported in this study  
574 are useful for relating CO<sub>2</sub> storage potential to rock/fluid interfacial tension. For instance,  
575 water-wet rocks are better for CO<sub>2</sub> storage (Iglauer et al., 2011) because of higher solid/CO<sub>2</sub>  
576 (solid = rock in this case) interfacial tension and oil-wet rocks exhibit poor CO<sub>2</sub>-storage  
577 potential in terms of structural and residual trapping (Iglauer et al., 2016) due to lower  
578 solid/CO<sub>2</sub> interfacial tension (e.g. pure quartz have higher solid/CO<sub>2</sub> interfacial tension than  
579 37% SiOH quartz, section 3.1). Physically, due to higher solid/CO<sub>2</sub> interfacial tension for water-  
580 wet rocks, CO<sub>2</sub> tends to stick to the rock (rock offers more resistance to the flow/leakage of  
581 buoyant CO<sub>2</sub>) and CO<sub>2</sub> is thus rendered immobile within the pores (leading to higher  
582 capillary/residual trapping in water-wet rocks; Iglauer et al., 2011). However, the detailed  
583 investigation of trapping potential must also account for solubility of CO<sub>2</sub> in the oil phase,  
584 sealing tendency of the caprock, and the pore geometry etc. to device suitable field scale storage  
585 plans.

586

587

588 **5. Conclusions**

589 We used Neumann's equation of state (Neumann et al., 1974) to compute the interfacial  
590 tensions of mineral/CO<sub>2</sub> and mineral/water systems for important rock forming minerals  
591 (quartz, water-wet mica and oil-wet mica) and for coals of high to low rank as a function of  
592 pressure, temperature and salinity. It was found that mineral/CO<sub>2</sub> interfacial tension decreased  
593 with pressure (consistent with Ameri et al. 2013 and Dickson et al. 2006), which is due to  
594 increased CO<sub>2</sub>-mineral intermolecular interactions (e.g. Iglauer et al., 2012, Al-Yaseri et al.  
595 2016b). It was also found that mineral/CO<sub>2</sub> interfacial tensions increased with temperature  
596 which is due to an increase in the difference of solid/CO<sub>2</sub> cohesive energies with temperature  
597 which thus leads to less favourable interactions between solid and CO<sub>2</sub> (thus higher  $\gamma_{sc}$ ).  
598 Moreover, the more non-wetting to water the surface was, the lower were the mineral/CO<sub>2</sub>  
599 interfacial tensions and the higher were the mineral/water interfacial tensions, e.g. oil-wet mica  
600 showed a lower mica/CO<sub>2</sub> interfacial tension than water-wet mica at the same pressure and  
601 temperature. Similarly, high rank coal had a lower coal/CO<sub>2</sub> interfacial tension than the low  
602 rank coal, because of greater hydrophobicity of high rank coal. This behaviour is attributed to  
603 fewer hydrophilic sites in high rank coal as opposed to abundance of hydrophilic sites in low  
604 rank coal (confirmed by IR spectroscopy). For all systems, solid/water interfacial tension  
605 decreased with temperature, except for quartz, where the quartz/water interfacial tension  
606 increased with temperature. The effect of salinity was also analysed and it was found that  
607 solid/water interfacial tension increased with salinity. Moreover, contact angles were predicted  
608 by Young's equation using the computed values of interfacial energies, and the predicted  $\theta$   
609 values were in good agreement with the experimental  $\theta$  values.

610 We conclude that the Neumann equation of state is adequate to quantify the solid surface  
611 energy and that the results demonstrated significant influence of surface energy in controlling  
612 the wettability dependence on pressure, temperature and salinity.

613

614

## 615 **References**

616

617 Al-Yaseri, A. Z., Lebedev, M., Barifcani, A., & Iglauer, S. (2016a). Receding and  
618 advancing (CO<sub>2</sub>+ brine+ quartz) contact angles as a function of pressure, temperature,  
619 surface roughness, salt type and salinity. *The Journal of Chemical Thermodynamics*, 93,  
620 416-423.



621 Al-Yaseri, A. Z., Roshan, H., Lebedev, M., Barifcani, A., & Iglauer, S. (2016b).  
622 Dependence of quartz wettability on fluid density. *Geophysical Research Letters*, 43(8),  
623 3771-3776.

624 Ameri, A., Kaveh, N. S., Rudolph, E. S. J., Wolf, K. H., Farajzadeh, R., & Bruining, J.  
625 (2013). Investigation on Interfacial Interactions among Crude Oil–Brine–Sandstone Rock–  
626 CO<sub>2</sub> by Contact Angle Measurements. *Energy & Fuels*, 27(2), 1015-1025.

627 Arif, M., Al-Yaseri, A. Z., Barifcani, A., Lebedev, M., & Iglauer, S. (2016a). Impact of  
628 pressure and temperature on CO<sub>2</sub>–brine–mica contact angles and CO<sub>2</sub>–brine interfacial  
629 tension: Implications for carbon geo-sequestration. *Journal of Colloid and Interface*  
630 *Science*, 462, 208-215.

631 Arif, M., Barifcani, A., Lebedev, M., & Iglauer, S. (2016b). Structural trapping capacity of  
632 oil-wet caprock as a function of pressure, temperature and salinity. *International Journal of*  
633 *Greenhouse Gas Control*, 50, 112-120.

634 Arif, M., Barifcani, A., Lebedev, M., & Iglauer, S. (2016c). CO<sub>2</sub>-wettability of low to high  
635 rank coal seams: Implications for carbon sequestration and enhanced methane recovery.  
636 *Fuel*, 181, 680-689.

637 Barton, A. F. (1991). *CRC handbook of solubility parameters and other cohesion*  
638 *parameters*. CRC press.

639 Blunt, M., Fayers, F. J., & Orr, F. M. (1993). Carbon dioxide in enhanced oil recovery.  
640 *Energy Conversion and Management*, 34(9), 1197-1204.

641 Broseta, D., Tonnet, N., & Shah, V. (2012). Are rocks still water-wet in the presence of  
642 dense CO<sub>2</sub> or H<sub>2</sub>S? *Geofluids*, 12(4), 280-294.

643 Brown, M. A., Huthwelker, T., Beloqui Redondo, A., Janousch, M., Faubel, M., Arrell, C.  
644 A., ... & van Bokhoven, J. A. (2012). Changes in the silanol protonation state measured in  
645 situ at the silica–aqueous interface. *The Journal of Physical Chemistry Letters*, 3(2), 231-  
646 235.

647 Bustin, R. M., & Clarkson, C. R. (1998). Geological controls on coalbed methane reservoir  
648 capacity and gas content. *International Journal of Coal Geology*, 38(1), 3-26.

649 Chen, C., Wan, J., Li, W., & Song, Y. (2015). Water contact angles on quartz surfaces  
650 under supercritical CO<sub>2</sub> sequestration conditions: Experimental and molecular dynamics  
651 simulation studies. *International Journal of Greenhouse Gas Control*, 42, 655-665.

652 Chiquet, P., Broseta, D., & Thibeau, S. (2007). Wettability alteration of caprock minerals  
653 by carbon dioxide. *Geofluids*, 7(2), 112-122.

654 Dickson, J. L., Gupta, G., Horozov, T. S., Binks, B. P., & Johnston, K. P. (2006). Wetting  
655 phenomena at the CO<sub>2</sub>/water/glass interface. *Langmuir*, 22(5), 2161-2170.

656 El-Maghraby, R. M., Pentland, C. H., Iglauer, S., & Blunt, M. J. (2012). A fast method to  
657 equilibrate carbon dioxide with brine at high pressure and elevated temperature including  
658 solubility measurements. *The Journal of Supercritical Fluids*, 62, 55-59.

659 Fowkes, F. M. (1964). Attractive forces at interfaces. *Industrial & Engineering Chemistry*,  
660 56(12), 40-52.

661 Fox, H. W., & Zisman, W. A. (1952). The spreading of liquids on low-energy surfaces. III.  
662 Hydrocarbon surfaces. *Journal of colloid science*, 7(4), 428-442.

663 Iglauer, S., Paluszny, A., Pentland, C. H., & Blunt, M. J. (2011). Residual CO<sub>2</sub> imaged  
664 with X-ray micro-tomography. *Geophysical Research Letters*, 38(21).

665 Iglauer, S., Mathew, M. S., & Bresme, F. (2012). Molecular dynamics computations of  
666 brine-CO<sub>2</sub> interfacial tensions and brine-CO<sub>2</sub>-quartz contact angles and their effects on  
667 structural and residual trapping mechanisms in carbon geo-sequestration. *Journal of colloid  
668 and interface science*, 386(1), 405-414.

669 Iglauer, S., Paluszny, A., & Blunt, M. J. (2013). Simultaneous oil recovery and residual gas  
670 storage: A pore-level analysis using in situ X-ray micro tomography. *Fuel*, 103, 905-914.

671 Iglauer, S., Pentland, C. H., & Busch, A. (2015a). CO<sub>2</sub> wettability of seal and reservoir  
672 rocks and the implications for carbon geo-sequestration. *Water Resources Research*, 51(1),  
673 729-774.

674 Iglauer, S., Al-Yaseri, A. Z., Rezaee, R., & Lebedev, M. (2015b). CO<sub>2</sub> wettability of  
675 caprocks: Implications for structural storage capacity and containment security.  
676 *Geophysical Research Letters*, 42(21), 9279-9284.

677 Iglauer, S., Rahman, T., Sarmadivaleh, M., Al-Hinai, A., Fernø, M. A., & Lebedev, M.  
678 (2016). Influence of Wettability on Residual Gas Trapping and Enhanced Oil Recovery in  
679 Three-Phase Flow: A Pore-Scale Analysis by Use of Microcomputed Tomography. *SPE  
680 Journal*.

681 IPCC, Working Group III of the Intergovernmental Panel on Climate Change, vol. 1, 2005,  
682 p. 443.

683 Janczuk, B., & Zdziennicka, A. (1994). A study on the components of surface free energy  
684 of quartz from contact angle measurements. *Journal of materials science*, 29(13), 3559-  
685 3564.

686 Javanbakht, G., Sedghi, M., Welch, W., & Goual, L. (2015). Molecular Dynamics  
687 Simulations of CO<sub>2</sub>/Water/Quartz Interfacial Properties: Impact of CO<sub>2</sub> Dissolution in  
688 Water. *Langmuir*, 31(21), 5812-5819.

689 Kittel, C. (2005). *Introduction to solid state physics*. Wiley.

690 Krevor, S., Pini, R., Zuo, L., & Benson, S. M. (2012). Relative permeability and trapping  
691 of CO<sub>2</sub> and water in sandstone rocks at reservoir conditions. *Water Resources Research*,  
692 48(2).

693 Krevor, S., Blunt, M. J., Benson, S. M., Pentland, C. H., Reynolds, C., Al-Menhali, A., &  
694 Niu, B. (2015). Capillary trapping for geologic carbon dioxide storage—From pore scale  
695 physics to field scale implications. *International Journal of Greenhouse Gas Control*, 40,  
696 221-237.

697 Kwok, D. Y., & Neumann, A. W. (1999). Contact angle measurement and contact angle  
698 interpretation. *Advances in colloid and interface science*, 81(3), 167-249.

699 Kwok, D. Y., & Neumann, A. W. (2000). Contact angle interpretation in terms of solid  
700 surface tension. *Colloids and Surfaces A: Physicochemical and Engineering Aspects*,  
701 161(1), 31-48.

702 Lackner, K. S. (2003). A guide to CO<sub>2</sub> sequestration. *Science*, 300(5626), 1677.

703 Li, D., & Neumann, A. W. (1992). Equation of state for interfacial tensions of solid-liquid  
704 systems. *Advances in Colloid and Interface Science*, 39, 299-345.

705 Li, X., Boek, E., Maitland, G. C., & Trusler, J. M. (2012a). Interfacial Tension of (Brines+  
706 CO<sub>2</sub>) : (0.864 NaCl+ 0.136 KCl) at Temperatures between (298 and 448) K, Pressures  
707 between (2 and 50) MPa, and Total Molalities of (1 to 5) mol· kg<sup>-1</sup>. *Journal of Chemical  
708 & Engineering Data*, 57(4), 1078-1088.

709 Liu, S., Yang, X., & Qin, Y. (2010). Molecular dynamics simulation of wetting behavior  
710 at CO<sub>2</sub>/water/solid interfaces. *Chinese Science Bulletin*, 55(21), 2252-2257.

711 Lun, Z., Fan, H., Wang, H., Luo, M., Pan, W., & Wang, R. (2012). Interfacial Tensions  
712 between Reservoir Brine and CO<sub>2</sub> at High Pressures for Different Salinity. *Energy & Fuels*,  
713 26(6), 3958-3962.

714 Manoj, B., Kunjomana, A. G., & Chandrasekharan, K. A. (2009). Chemical leaching of  
715 low rank coal and its characterization using SEM/EDAX and FTIR. *Journal of Minerals  
716 and Materials Characterization and Engineering*, 8(10), 821.

717 McCaughan, J., Iglauer, S., & Bresme, F. (2013). Molecular dynamics simulation of  
718 water/CO<sub>2</sub>-quartz interfacial properties: application to subsurface gas injection. *Energy*  
719 *Procedia*, 37, 5387-5402.

720 Neumann, A. W., Good, R. J., Hope, C. J., & Sejpal, M. (1974). An equation-of-state  
721 approach to determine surface tensions of low-energy solids from contact angles. *Journal*  
722 *of Colloid and Interface Science*, 49(2), 291-304.

723 Owens, D. K., & Wendt, R. C. (1969). Estimation of the surface free energy of polymers.  
724 *Journal of applied polymer science*, 13(8), 1741-1747.

725 Roshan, H., Al-Yaseri, A. Z., Sarmadivaleh, M., & Iglauer, S. (2016). On wettability of  
726 shale rocks. *Journal of colloid and interface science*, 475, 104-111.

727 Saraji, S., Piri, M., & Goual, L. (2014). The effects of SO<sub>2</sub> contamination, brine salinity,  
728 pressure, and temperature on dynamic contact angles and interfacial tension of supercritical  
729 CO<sub>2</sub>/brine/quartz systems. *International Journal of Greenhouse Gas Control*, 28, 147-155.

730 Sarmadivaleh, M., Al-Yaseri, A. Z., & Iglauer, S. (2015). Influence of temperature and  
731 pressure on quartz–water–CO<sub>2</sub> contact angle and CO<sub>2</sub>–water interfacial tension. *Journal of*  
732 *colloid and interface science*, 441, 59-64.

733 Sarwar, A., Khan, M. N., & Azhar, K. F. (2012). Coal chemistry and morphology of thar  
734 reserves, Pakistan. *Journal of Minerals and Materials Characterization and Engineering*,  
735 11(08), 817.

736 Schaeff, H. T., & McGrail, B. P. (2004). Direct measurements of pH in H<sub>2</sub>O-CO<sub>2</sub> brine  
737 mixtures to supercritical conditions. In *Proceedings of the 7th International Conference on*  
738 *Greenhouse Gas Control Technologies (GHGT-7)*.

739 Shojai Kaveh, N. S., Wolf, K. H., Ashrafizadeh, S. N., & Rudolph, E. S. J. (2012). Effect  
740 of coal petrology and pressure on wetting properties of wet coal for CO<sub>2</sub> and flue gas  
741 storage. *International Journal of Greenhouse Gas Control*, 11, S91-S101.

742 Shojai Kaveh, N., Barnhoorn, A., & Wolf, K. H. (2016). Wettability evaluation of silty  
743 shale caprocks for CO<sub>2</sub> storage. *International Journal of Greenhouse Gas Control*, 49, 425-  
744 435.

745 Socrates, G. (2004). *Infrared and Raman characteristic group frequencies: tables and charts*.  
746 John Wiley & Sons.

747 Staszczuk, P. (1989). On the determination of surface free energy of coal by means of the  
748 derivatograph. *Fuel science & technology international*, 7(1), 89-101.

749 Siemons, N., Bruining, H., Castelijns, H., & Wolf, K. H. (2006). Pressure dependence of  
750 the contact angle in a CO<sub>2</sub>-H<sub>2</sub>O-coal system. *Journal of Colloid and Interface Science*,  
751 297(2), 755-761.

752 Tadmor, R. (2004). Line energy and the relation between advancing, receding, and young  
753 contact angles. *Langmuir*, 20(18), 7659-7664.

754 Tripp, C. P., & Combes, J. R. (1998). Chemical modification of metal oxide surfaces in  
755 supercritical CO<sub>2</sub>: The interaction of supercritical CO<sub>2</sub> with the adsorbed water layer and  
756 the surface hydroxyl groups of a silica surface. *Langmuir*, 14(26), 7348-7352.

757 Van Oss, C. J., Good, R. J., & Chaudhury, M. K. (1986). The role of van der Waals forces  
758 and hydrogen bonds in "hydrophobic interactions" between biopolymers and low energy  
759 surfaces. *Journal of colloid and Interface Science*, 111(2), 378-390.

760 Wu, S. (1971, January). Calculation of interfacial tension in polymer systems. In *Journal*  
761 *of Polymer Science Part C: Polymer Symposia* (Vol. 34, No. 1, pp. 19-30). Wiley  
762 Subscription Services, Inc., A Wiley Company.

763 Wu, D., Liu, G., & Sun, R. (2014). Investigation on structural and thermodynamic  
764 characteristics of perhydrous bituminous coal by fourier transform infrared spectroscopy  
765 and thermogravimetry/mass spectrometry. *Energy & Fuels*, 28(5), 3024-3035.

766 Żenkiewicz, M. (2007). Methods for the calculation of surface free energy of solids. *Journal*  
767 *of Achievements in Materials and Manufacturing Engineering*, 24(1), 137-145.